

Journal of Geophysical Research: Atmospheres

RESEARCH ARTICLE

10.1002/2014JD022779

Key Points:

- Climatology of vertical distributions of cloud LWC, IWC, and cloud fraction
- Geographical and seasonal variations of cloud properties for eight cloud types
- Relation between large-scale parameters and cloud vertical structure

Correspondence to:L. Huang,
Lei.Huang@jpl.nasa.gov**Citation:**

Huang, L., J. H. Jiang, Z. Wang, H. Su, M. Deng, and S. Massie (2015), Climatology of cloud water content associated with different cloud types observed by A-Train satellites, *J. Geophys. Res. Atmos.*, 120, 4196–4212, doi:10.1002/2014JD022779.

Received 29 OCT 2014

Accepted 10 APR 2015

Accepted article online 15 APR 2015

Published online 11 MAY 2015

Climatology of cloud water content associated with different cloud types observed by A-Train satellites

Lei Huang¹, Jonathan H. Jiang¹, Zhien Wang², Hui Su¹, Min Deng², and Steven Massie³

¹Jet Propulsion Laboratory, California Institute of Technology, Pasadena, California, USA, ²Department of Atmospheric Science, University of Wyoming, Laramie, Wyoming, USA, ³Laboratory for Atmospheric and Space Physics, University of Colorado Boulder, Boulder, Colorado, USA

Abstract This study investigates the climatology of vertical distributions of cloud liquid water content, ice water content, and cloud fraction (CFR) associated with eight different cloud types, by utilizing the combined CloudSat radar and Cloud-Aerosol Lidar and Infrared Pathfinder Satellite Observations lidar measurements. The geographical and seasonal variations of these cloud properties for each cloud type are also analyzed. The cloud water content (CWC) of each cloud type is sorted by three parameters obtained from colocated satellite observations to investigate the relationships between large-scale conditions and the vertical structure of clouds. Results show that different cloud types have different altitudes of CWC and CFR peaks, and the altitude of CFR peak does not always overlap with that of CWC peak. Each type of cloud shows a clear asymmetric pattern of spatial distribution between Northern Hemisphere (NH) and Southern Hemisphere (SH). Stratocumulus and stratus clouds make the greatest contribution to the liquid water path, while the ice water path is mostly contributed by deep convective cloud over the tropics and nimbostratus over the middle and high latitudes. Over both middle and high latitudes, clouds have larger seasonal variation in the NH than in the SH. Over ocean, large CWCs of deep convective cloud, cirrus, and altostratus are above 7 km, and are associated with high convective available potential energy ($>2000\text{ J/kg}$), warm sea surface temperature ($>303\text{ K}$), and relatively high precipitation ($>1\text{ mm/h}$). Over land, most of the middle and high clouds have similar CWC distributions compared to those over ocean, but altocumulus and low clouds are quite different from those over ocean.

1. Introduction

As an important component of the climate system, clouds play a critical role in the global hydrological cycle and Earth's energy budget. Both ice and liquid clouds have significant impacts on the radiation budget through their shortwave albedo (reflection of solar radiation) and longwave greenhouse (absorption of longwave) radiation effects [e.g., Harrison *et al.*, 1990; Randall and Tjemkes, 1991]. To the first order, clouds and their properties are determined by general circulation. However, clouds also have significant feedbacks on the atmospheric circulation and climate through various dynamic and thermodynamic processes [Stephens, 2005; Bony *et al.*, 2006]. Currently, clouds remain as one of the largest sources of uncertainty in climate projections [e.g., Andrews *et al.*, 2012; Su *et al.*, 2014]. To reduce the cloud uncertainty, we need long-term and high-resolution cloud observations from both surface- and satellite-based remote sensors to constrain model simulations, and develop more accurate climate models with higher spatiotemporal resolution and better cloud parameterizations to resolve cloud processes in subgrid scales.

The vertical distribution of clouds is important in determining the cloud radiative forcing. Many active and passive sensors have traditionally been used to obtain cloud information from both the ground and space [e.g., Sassen, 1984, 1991; Rossow and Schiffer, 1999; Lazarus *et al.*, 2000; Dong *et al.*, 2006]. In general, active sensors (e.g., lidar and radar) can provide vertically resolved cloud properties (e.g., ice/liquid water content), while passive sensors, such as the Moderate Resolution Imaging Spectroradiometer (MODIS), can measure column-integrated cloud properties (e.g., ice/liquid water path) [Wang and Sassen, 2001]. New information about the vertical distribution of clouds from satellite observations has become available since 2006, when CloudSat and Cloud-Aerosol Lidar and Infrared Pathfinder Satellite Observations (CALIPSO) joined the A-Train satellite constellation [L'Ecuyer and Jiang, 2010]. The synergy of these active remote sensors along with other A-Train sensors has provided colocated and near-simultaneous measurements

that have been widely used for climate studies and model evaluations [e.g., *Stephens et al.*, 2008; *Li et al.*, 2011; *Chen et al.*, 2011; *Su et al.*, 2011, 2013; *Jiang et al.*, 2012; *Huang et al.*, 2012, 2014].

Different types of clouds have distinctive microphysical properties controlled by various cloud dynamic processes, resulting in different cloud radiative forcings [e.g., *Hartmann et al.*, 1992]. *Chen et al.* [2000] found that cloud-type variations are as important as cloud cover in modifying the radiation field of the Earth-atmosphere system, and each cloud type has different radiative impact at the top-of-atmosphere and surface. It is a great challenge to accurately predict future climate change without the appropriate representation of the processes and feedback mechanisms that control different cloud types and their properties in climate models. Therefore, classifying clouds into different types is an important task for cloud remote sensing and global cloud climatology studies. Based on passive measurements, the International Satellite Cloud Climatology Project classified clouds into nine different types according to the combination of cloud top pressure and cloud optical thickness: low clouds (cumulus (Cu), stratocumulus (Sc), and stratus (St)), middle clouds (altocumulus (Ac), altostratus (As), and nimbostratus (Ns)), and high clouds (cirrus, cirrostratus, and deep convective cloud (Dc)) [*Rossow and Schiffer*, 1999]. *Wang and Sassen* [2001] developed a new approach to classify clouds into eight types by combining ground-based lidar, radar, and radiometer measurements at the Atmospheric Radiation Measurement Climate Research Facility site. This lidar-radar based cloud classification scheme took full advantage of cloud vertical and spatial structure and was modified for CloudSat and CALIPSO observations to provide global cloud-type distributions, which are now available from two CloudSat Products (2B-CLDCLASS and 2B-CLDCLASS-LIDAR) [*Sassen and Wang*, 2008, 2012]. With 1 year CloudSat radar-only data, *Austin et al.* [2009] reported the annual mean ice water path (IWP) of different cloud types and found that the majority of atmospheric ice mass is contributed by As, Ns, and Dc.

Previous studies have used cloud ice water content (IWC) and liquid water content (LWC) observed by A-Train satellites for climate model evaluations [e.g., *Li et al.*, 2005, 2012; *Waliser et al.*, 2009; *Eliasson et al.*, 2011; *Jiang et al.*, 2012; *Su et al.*, 2013], and these studies have shown large model errors in simulating both ice and liquid clouds. However, specifically identifying whether the model errors are coming primarily from the convective or the stratiform cloud scheme remains a challenge. A cloud-type climatology study can help to isolate the specific physical processes that could be the source of the largest model errors and to separate clouds associated with convection from those formed by large-scale processes.

In this study, we analyze the climatological vertical distribution of cloud water content (CWC, the sum of LWC and IWC) and cloud fraction (CFR) of different cloud types by using combined CloudSat radar and CALIPSO lidar observations, and investigate the relationships between large-scale environmental conditions and the vertical distributions of different cloud types. A brief description of CloudSat/CALIPSO measurements, data, and methodology used is given in section 2. The climatological vertical profiles of CWC and CFR associated with different cloud types, their geographical, and seasonal variations are presented and discussed in section 3. Section 4 discusses the relationships between large-scale environmental conditions and the vertical distributions of different cloud types. Major findings and conclusions from this study are summarized in section 5.

2. Data and Methodology

In this study, cloud LWC and corresponding cloud type data are from CloudSat 2B-CWC-RO and 2B-CLDCLASS product, respectively, which are radar-only data. Cloud IWC, cloud fraction, and corresponding cloud type data are from CloudSat 2B-ICE and 2B-CLDCLASS-LIDAR products, which are generated by combining CloudSat radar and CALIPSO lidar measurements.

The CloudSat and CALIPSO satellites were launched together into a Sun-synchronous orbit in April 2006 with an equator-crossing time of 1:30 P.M. and 1:30 A.M. Both satellites fly in formation as part of the A-Train satellite constellation [*L'Ecuyer and Jiang*, 2010]. The main instrument on board CloudSat is a 94 GHz cloud profiling radar (CPR) which measures vertical structures of clouds and precipitation [*Stephens et al.*, 2002]. The CPR has a minimum sensitivity of ~ -30 dBZ_e with ~ 480 m effective vertical resolution, but the measurements are reported on an increment of ~ 240 m with 125 vertical layers. The footprint for a single profile is approximately 1.3 km across-track by 1.7 km along-track, with along-track sampling spaced every 1.1 km [*Stephens et al.*, 2008]. One primary instrument on board the CALIPSO is the Cloud-Aerosol

Table 1. The Eight Cloud Types Defined by CloudSat 2B-CLDCLASS and 2B-CLDCLASS-LIDAR Product^a

Dc	Deep convective cloud
Ci	Cirrus, Cirrostratus, and Cirrocumulus
Ns	Nimbostratus
As	Altocstratus
Ac	Altocumulus
Cu	Cumulus
St	Stratus
Sc	Stratocumulus

^aThe left column lists the abbreviation of each cloud type, and the right column lists the full name of each cloud type.

Lidar with Orthogonal Polarization (CALIOP), which is a dual wavelength polarization lidar designed to acquire vertical profiles of attenuated backscatter during both daytime and nighttime [Winker *et al.*, 2007]. CALIOP provides high-resolution (60 m vertical and 1 km horizontal resolution between 8.2 and 20.2 km; 30 m vertical and 333 m horizontal resolution below 8.2 km) profiles of cloud and aerosol measurements

[Winker *et al.*, 2007; Huang *et al.*, 2013]. The different working wavelengths of CALIOP and CPR allow them to provide complementary observations. As shown by previous studies [e.g., Wang and Sassen, 2001; Deng *et al.*, 2010], lidar cannot penetrate optically thick low and midlevel clouds because of strong optical attenuation, but can accurately detect most midlevel and high-level clouds which are often optically thin (e.g., altocumulus and cirrus clouds); on the other hand, radar can penetrate thick clouds to detect many midlevel and low-level clouds. Therefore, combining lidar and radar measurements can provide more reliable cloud properties [e.g., Sassen *et al.*, 2009; Mace *et al.*, 2009].

Previous validation studies [e.g., Heymsfield *et al.*, 2008; Eriksson *et al.*, 2008; Barker *et al.*, 2008; Austin *et al.*, 2009] have indicated that the CloudSat IWC/LWC retrieval error is within ~50% and have a factor of 2 uncertainty. The CloudSat and CALIPSO combined Level-2C ice cloud property product (2C-ICE) [Deng *et al.*, 2010, 2013] and Level-2B cloud classification product (2B-CLDCLASS-LIDAR) [Wang *et al.*, 2013] are two standard CloudSat data sets that are publicly available at the CloudSat data processing center since 2012. The 2C-ICE product provides a vertically resolved retrieval of ice cloud properties (e.g., effective radius, IWC, and visible extinction) by synergistically combining CloudSat and CALIPSO observations at the CloudSat horizontal and vertical resolutions based on an optimal estimation framework. More details of retrieval algorithms and assumptions can be found in Deng *et al.* [2010]. It is worthwhile to point out that the previous 2C-ICE data had some problems in year 2009/2010 due to an algorithm bug in the lidar-only region, and it is fixed in the newly reprocessed data that we use in this study. The uncertainty of 2C-ICE IWC is around 30% [Deng *et al.*, 2013]. The 2B-CLDCLASS-LIDAR product classifies cloud scenarios into eight types (Table 1) by using vertical and horizontal cloud properties, the presence or absence of precipitation, cloud temperature, and upward radiance from MODIS measurements. The class of high cloud includes cirrus, cirrocumulus, and cirrostratus, and the class of Cu cloud represents cumulus congestus and fair weather cumulus [Wang *et al.*, 2013]. A cloud type is assigned to each cloud layer, so clouds in a single radar profile may be partitioned into several types, contributing to several different CWC profiles. Besides cloud type, the 2B-CLDCLASS-LIDAR data also provide other cloud layer information including cloud layer top and base height, cloud fraction and cloud phase. We use the LWC from CloudSat 2B-CWC-RO product and corresponding cloud-type information from CloudSat 2B-CLDCLASS product. These two products are generated using radar-only retrieval [Austin *et al.*, 2009]. There are several issues need to be noted about the radar-only retrieval: First, CloudSat radar-only retrieval may miss low-level clouds or clouds with small droplets [Sassen and Wang, 2008]. Although lidar can partly solve this problem, currently there are no LWC data from radar-lidar combined products. Estimating the impact of missing cloud LWC by radar needs more future work and is beyond the scope of this study. Second, precipitation could affect the radar-only retrieval of LWC profiles (<http://www.cloudsat.cira.colostate.edu/datalissue.php?prodid=70&pvid=201&anomalyid=325229>). Thus, the retrieved LWC in the 2B-CWC-RO product is screened by removing these cloud profiles where surface precipitation is detected using the precipitation flags in the CloudSat 2C-PRECIP-COLUMN product [Haynes *et al.*, 2009], although this may cause an underestimation of cloud LWC [Eliasson *et al.*, 2011; Jiang *et al.*, 2012]. Third, the 2B-CWC-RO product uses a temperature-dependent CWC partition for clouds with temperature between 0°C and -20°C [Austin *et al.*, 2009]. If a cloud measurement is identified as cirrus cloud at -20°C, the 2B-CWC-RO algorithm will generate both LWC and IWC, while the 2C-ICE algorithm assumes radar measurements are dominated by ice and provides only ice retrievals. Such limitations can be relieved when new cloud products with

improved algorithms are released in the future. In addition, CloudSat measurements within the lowest kilometer are affected by ground contamination [Mace *et al.*, 2007; Sassen and Wang, 2008], thus we limit our analysis to cloud profiles above 1 km.

In this study, the time period for all the CloudSat data sets is from January 2007 to December 2010. For the IWC of each cloud profile, first we identify the number of cloud layers, and the cloud type for each layer. Then we regrid each cloud layer to vertical bins at 500 m interval using cloud layer base and top altitude from 2B-CLDCLASS-LIDAR data. The IWC for each 500 m bin is calculated from 2C-ICE, and the cloud fraction is from 2B-CLDCLASS-LIDAR. For LWC, it is much easier than IWC calculation because 2B-CLDCLASS is a profile data with the same vertical resolution as 2B-CWC-RO. Thus, we only need to link LWC with cloud type at each 500 m vertical bin from these two products. The cloud liquid water path (LWP) and ice water path (IWP) are calculated as the integration of cloud LWC and IWC of all layers, respectively. We average all the 4 year cloud data (including both cloud and clear-sky) to get the climatological mean of cloud properties (LWC, IWC, LWP, IWP, and CFR) associated with each cloud type, over a specific region or each 4° latitude \times 8° longitude grid box.

Several colocated measurements from other satellites are also used together with the cloud observations. The sea surface temperature (SST) data from the Advanced Microwave Scanning Radiometer (AMSR-E) aboard Aqua are obtained from the Remote Sensing Systems (<http://www.remss.com>). The AMSR-E instrument has a noise of 0.1 K, which leads to a SST uncertainty of about 0.2°C [Gentemann *et al.*, 2010]. The SST data have a resolution of $0.25^\circ \times 0.25^\circ$. The atmospheric temperature and water vapor profiles are measured by the Atmospheric Infrared Sounder (AIRS) aboard Aqua. The AIRS instrument suite was designed to provide tropospheric temperature retrieval with an uncertainty of 1.0 K over 1 km layers, and water vapor retrieval with an uncertainty of 10% over 2 km layers [Fetzer *et al.*, 2003]. We use the standard AIRS Level 3 product (with a horizontal resolution of $1^\circ \times 1^\circ$) to calculate the convective available potential energy (CAPE) twice a day, based on an assumption that an air parcel is lifted pseudoadiabatically from 1000 hPa. We also use the 3B42 3-hourly precipitation data from the Tropical Rainfall Measuring Mission (TRMM) with a resolution of $0.25^\circ \times 0.25^\circ$ [Huffman *et al.*, 2007]. The uncertainty of the TRMM precipitation data is estimated at 90%–120% for light rain (<0.25 mm/h) and 20%–40% for heavy rain [Habib and Krajewski, 2002; Aghakouchak *et al.*, 2009]. All these parameters (SST, CAPE, and precipitation) are interpolated onto the CloudSat tracks in both space and time. We define 25 bins for each parameter and 50 altitude bins (500 m interval) above mean sea level. For each cloud type, we calculate the average of the CWC within each altitude (y axis) – parameter (x axis) grid box as the sum of CWC associated with this cloud type divided by the total number of CloudSat measurements (including clear-sky) within the same grid box. We perform this conditional sampling analysis for land and ocean area separately over three tropical zones (30°S – 15°S , 15°S – 15°N , and 15°N – 30°N) for year 2007. The total number of cloud profiles used is ~ 40 million.

3. Climatology of Different Cloud Types

3.1. Vertical Distribution of Cloud Water Content and Fraction

3.1.1. Tropical Mean Profiles

First, we calculate the climatological cloud LWC, IWC, CWC, and cloud fraction profiles over the tropics (30°S – 30°N). The results are shown in Figure 1 for each cloud type and all types of cloud combined. The altitude starts from 1 km above mean sea level (hereinafter). We combine the St and Sc clouds (use “Sc” to denote hereinafter) because it is difficult to distinguish these similar low-level clouds in view of current CPR signal contamination in the lowest several vertical bins above the surface [Sassen and Wang, 2008]. We use “Ci” to denote the class of high cloud which includes cirrus, cirrocumulus, and cirostratus. “Cu” cloud represents cumulus congestus and fair weather cumulus. In general, the ice-dominant clouds include As, Ns, Ci, and Dc, while the liquid-dominant clouds include Ac and Sc. Some types of cloud have mixed phases, and the composition is complicated. For example, liquid phase dominates below 3 km for Ns, below 4.5 km for As, and below 4 km for Cu; while ice phase dominates above 7 km for Ac and above 4 km for Cu. Besides, there are warm liquid cloud droplets in the lower level of Dc, but the LWC is less than 0.1 mg/m^3 . Generally, liquid clouds are located below 8 km, while ice clouds can reach as high as 17 km.

The vertical distributions of CWC and CFR show large differences among all cloud types (Figure 1). For the high clouds, Dc has a wide CWC peak from 5 km to 12 km with a magnitude of $\sim 10 \text{ mg/m}^3$, while the CWC

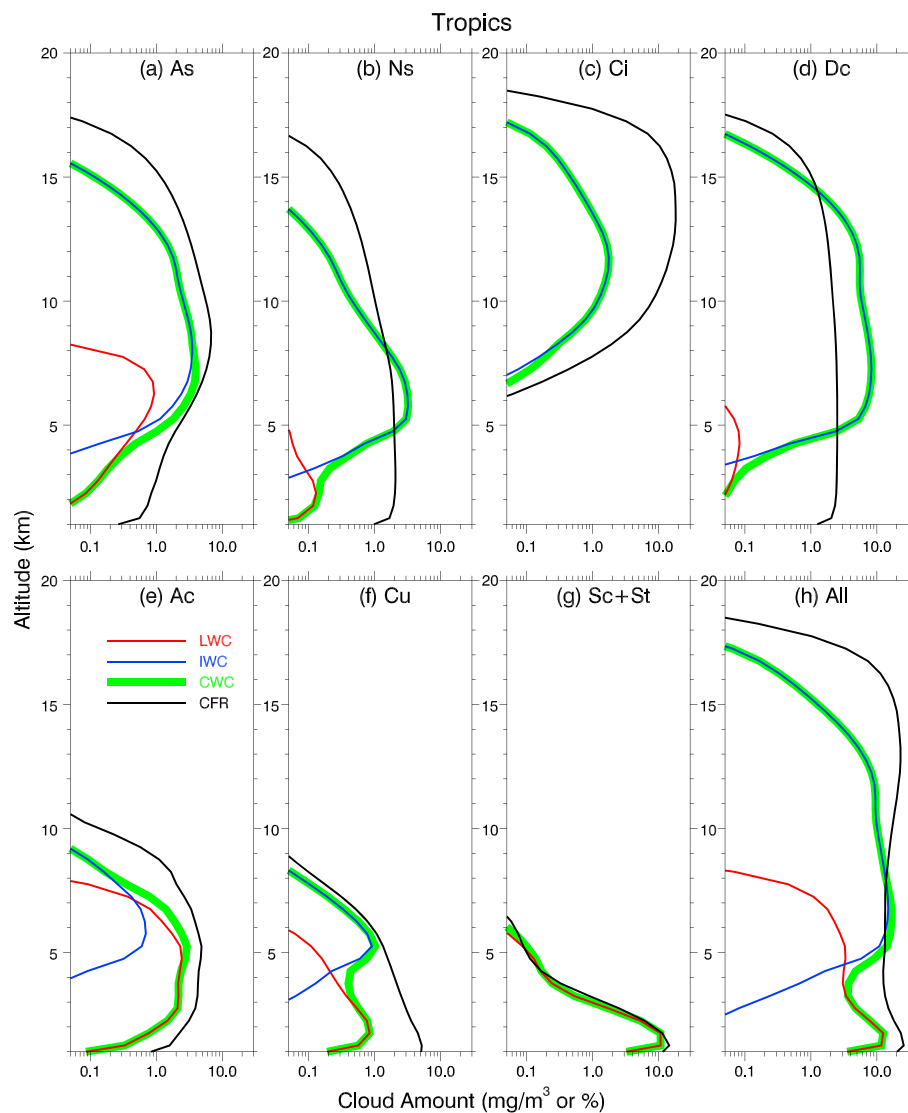


Figure 1. Vertical profiles of annual average cloud water content and cloud fraction from 4 year CloudSat/CALIPSO observations over the tropics (30°S - 30°N) for (a) altostratus, (b) nimbostratus, (c) cirrus, cirrocumulus, and cirrostratus combined, (d) deep convective cloud, (e) altocumulus, (f) cumulus, (g) stratocumulus and stratus combined, and (h) all types of cloud combined. The red curve represents liquid water content (LWC, mg/m^3), blue curve represents ice water content (IWC, mg/m^3), green curve represents cloud water content (CWC, mg/m^3), and black curve represents cloud fraction (CFR, %).

of Ci peaks at ~ 12 km with a magnitude of $\sim 1 \text{ mg}/\text{m}^3$. For the middle clouds, the CWC peaks are between 5 km and 7 km. The CWC of Ac peaks at a lower altitude with a smaller value than that of As and Ns. The maximum CWC values of these three types are $\sim 3\text{--}4 \text{ mg}/\text{m}^3$. Besides, the CWC of Ac is less than $0.05 \text{ mg}/\text{m}^3$ above 9 km, while As and Ns clouds can have CWC larger than this value above 13 km (i.e., a much higher vertical extent). For the low clouds, the CWC of Sc reaches maximum near the surface at 1–2 km with a magnitude of $\sim 10 \text{ mg}/\text{m}^3$, contributed purely by liquid droplets; the CWC of Cu shows two peaks, one at ~ 2 km contributed by liquid and the other at ~ 5.5 km contributed by ice. However, both peak values of Cu are one order of magnitude smaller than that of Sc. The all-types-combined (Figure 1h) CWC profile shows two peaks: the one at 1–2 km is mainly contributed by Sc and the other one at 5–12 km is mostly contributed by Dc. The CFR profiles of some cloud types are similar to the corresponding CWC profiles, such as Ci, As, Ac, and Sc. For other cloud types, the CFR and CWC profiles are quite different. For example, the CFR of Dc is almost constant from near surface to ~ 15 km, although it is only $\sim 2.5\%$. This is mainly due to its relatively low occurrence frequency and small areal extent. The CFR of Cu, including

trade Cu and fair weather Cu, peaks near the boundary layer (~5.2%) and decreases rapidly with altitude. Cumulus congestus can develop deep in vertical extent, but its occurrence frequency is much lower. Ci has the maximum CFR of 18% among the high clouds, As has the maximum CFR of 7% among the middle clouds, and Sc has the maximum CFR of 14% among the low clouds.

3.1.2. Zonal Mean Profiles

Next, we calculate the zonal average of LWC, IWC, and CWC for each cloud type, and the results are shown in Figure 2. In general, a clear asymmetric distribution exists between Northern Hemisphere (NH) and Southern Hemisphere (SH) for nearly all types of cloud. For the high clouds, LWC is negligible over all latitudes, while IWC reaches maximum over the tropics due to the stronger convective activities. Ice clouds are denser and can reach a higher altitude over the Northern Hemispheric tropics than south of the equator. This is mainly due to the atmospheric circulation differences related to the different arrangement of land and ocean in the two hemispheres and the seasonal shift in the location of the Intertropical Convergence Zone (ITCZ) [Rossow and Schiffer, 1999]. For the middle clouds, the maximum LWC and IWC mainly occur over middle-high latitudes of both hemispheres. However, As and Ac also have CWC peak values over the tropics. The IWC of all three types (Ns, As, and Ac) is larger over the middle-high latitudes of SH than NH. As and Ac also have larger IWC over the NH tropics than over the SH tropics. Ns has minimum CWC over the tropics and maximum CWC near surface over SH high latitudes which is mostly contributed by ice. For the low clouds, Cu has LWC peak over the SH subtropics (5–20°S) and IWC peak over midlatitude (40–50°S); Sc has LWC peak (~20 mg/m³) over the SH extratropics (20–50°S) and small IWC values (~5 mg/m³) in the polar regions (beyond 50°S or 50°N). In the NH, the CWC values of both Cu and Sc are much smaller than those over the same latitudes in the SH. For all-types-combined clouds, the LWC distribution resembles that of Sc, while the IWC distribution resembles the combination of Dc and Ns; the vertical distribution of zonal mean CWC is similar to that shown in Figure 1 of Su *et al.* [2008].

3.2. Geographical Distribution of Cloud Water Path

Figure 3 displays the 4 year mean geographical distributions of cloud LWP and IWP for each cloud type. Over the globe, the LWP is mostly contributed by Sc clouds, while the IWP is mostly contributed by Dc over the tropics and Ns over the middle and high latitudes. The high clouds (especially Ci) have the smallest LWP, while Sc clouds have the largest LWP. In fact, the nonzero LWPs of Ci shown in Figure 3b are mainly due to the temperature-dependent liquid-ice partition used in the 2B-CWC-RO product. Ac has the second largest magnitude of LWPs, especially over the tropical convective regions. Both As and Ac show relatively large LWPs over the middle and high latitudes, which may relate to the synoptic-scale lifting of water vapor into middle level. Both Ns and Cu show a LWP center over the Tibetan Plateau, indicating frequent convective activities over this region during boreal summer. The Sc clouds have several LWP centers located over the subtropical subsidence regions, such as the eastern Pacific, southern Atlantic, and south Indian Ocean. Over these regions, other types of clouds generally have minimum LWPs and very low occurrence frequency.

The largest IWP values are associated with As, Ns, and Dc clouds. However, the locations of the heaviest burden for these three types are quite different. Dc has the maximum IWPs over the convective region in the tropics; Ns has the maximum IWPs over the middle-high latitude storm tracks associated with synoptic weather systems. The distribution of large IWPs of As resembles a combination of Dc and Ns, although the magnitude is much smaller than the other two types, suggesting that As developments are closely linked to these two types of cloud. In fact, deep precipitating clouds or thick clouds with base below 2 km are classified as Dc or Ns, while deep clouds with base above 2 km are often classified as As. The contribution by Ci to the global ice amount is small, and its large IWPs have similar distribution to those of Dc, suggesting the detrainment of ice at the top of Dc plays an important role in the formation and distribution of Ci. The IWPs of Ac, Cu, and Sc have comparable magnitude, and the large values are mainly located over the high latitudes (especially the oceanic regions).

3.3. Seasonal Variation of Cloud Water Content and Fraction

The seasonal variations of cloud water content and cloud fraction associated with each cloud type over different latitudinal bands are shown in Figure 4. The solid and dotted lines indicate CWC and CFR, respectively. Different colors represent different seasons. Over the tropics (30°S–30°N), all types of cloud

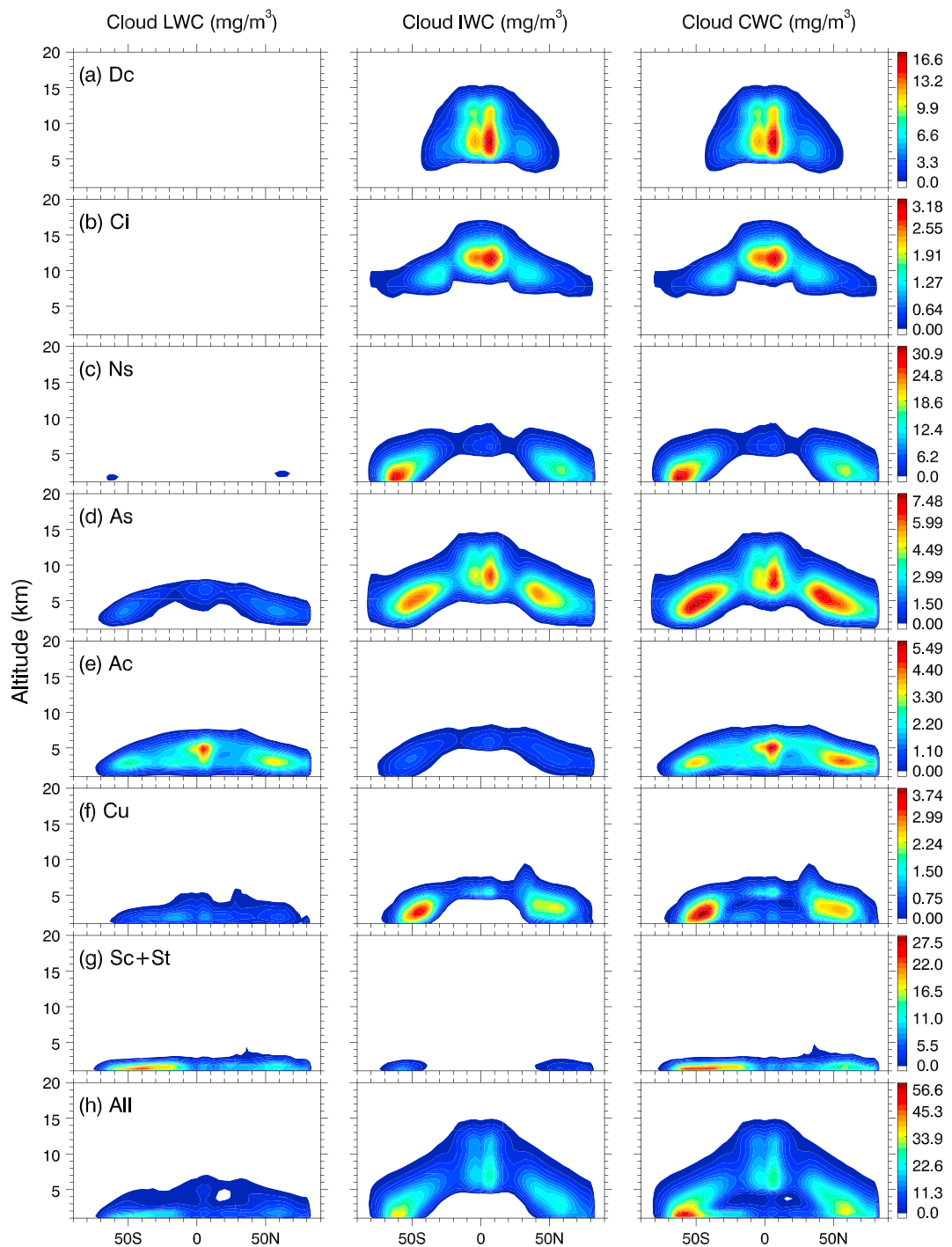


Figure 2. Vertical distributions of zonal average of (left) LWC (mg/m³), (middle) IWC (mg/m³), and (right) CWC (mg/m³) for each cloud type: (a) deep convective cloud, (b) cirrus, cirrocumulus and cirostratus combined, (c) nimbostratus, (d) altostratus, (e) altocumulus, (f) cumulus, (g) stratocumulus and stratus combined, and (h) all types of cloud combined.

show little seasonal variation of CWC and CFR. Over the midlatitudes (30–60°N or 30–60°S), clouds have larger seasonal variation in the NH than in the SH because of larger landmass in the NH. Generally, ice clouds (Dc, Ci, As, and Ac) have larger seasonal variation in the upper level than in the lower level. During wet season (i.e., June–July–August (JJA) in the NH, December–January–February (DJF) in the SH), both CWC and CFR of these ice clouds are larger than other seasons, due to more frequent and stronger convective

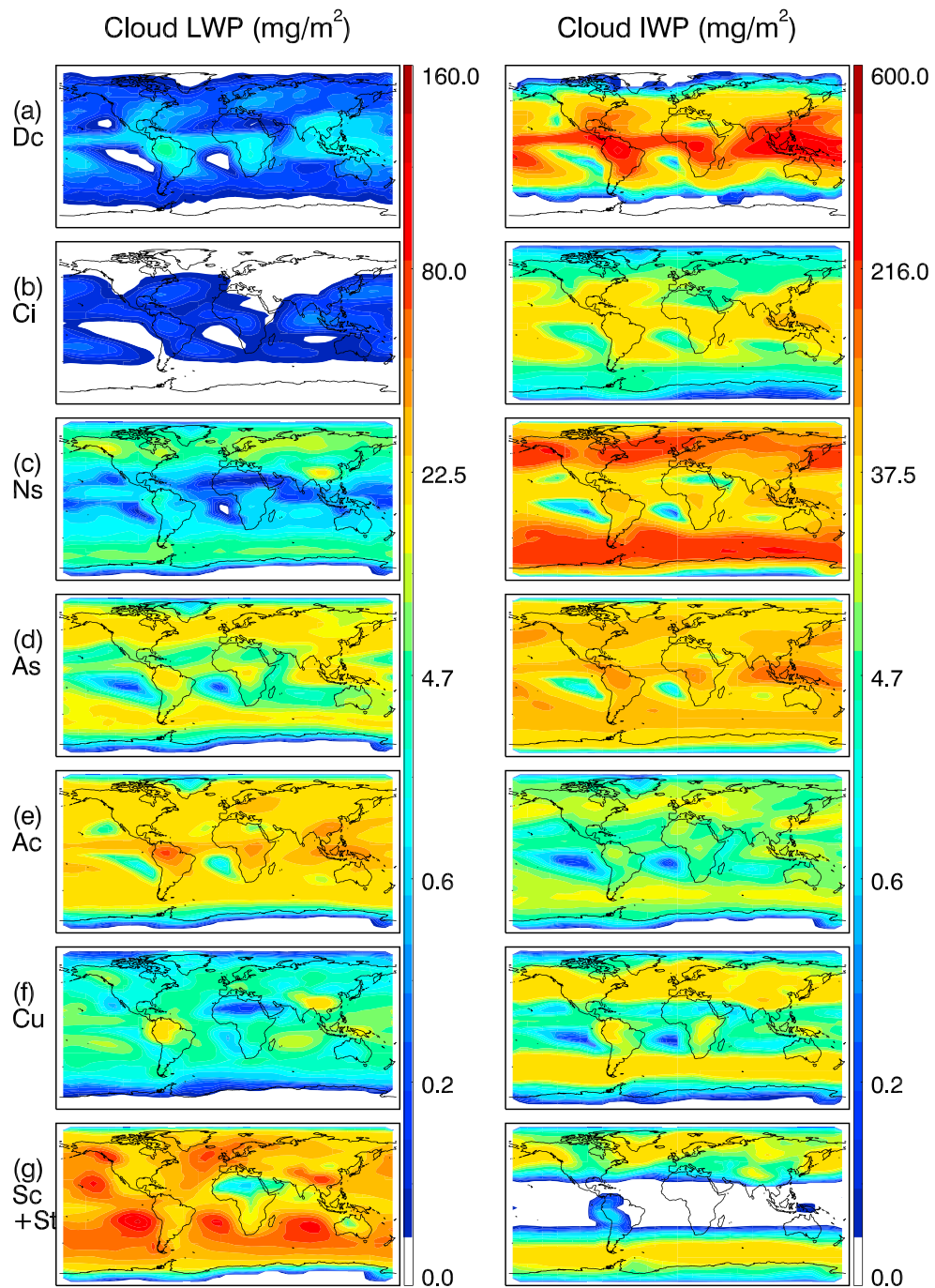


Figure 3. Geographical distributions of 4 year average of (left) liquid water path (mg/m^2) and (right) ice water path (mg/m^2) for each cloud type: (a) deep convective cloud, (b) cirrus, cirrocumulus, and cirrostratus combined, (c) nimbostratus, (d) altostratus, (e) altocumulus, (f) cumulus, and (g) stratocumulus and stratus combined.

activities that produce more ice in the upper level. Ns and Cu clouds have larger seasonal variation below 5 km, where most ice/liquid mass are concentrated. The seasonal differences of CWC for Ns and Cu reach maximum near the surface and decrease with altitude. However, Cu over NH midlatitude is an exception. Above 5 km, Cu also has large seasonal variation over this region, which may be related to the monsoon activities. Sc clouds have little seasonal variation below 5 km. Although Sc appears to have some seasonal variation above 5 km in the NH, the CWC magnitude is less than 0.4 mg/m^3 due to very low occurrence frequency above this level.

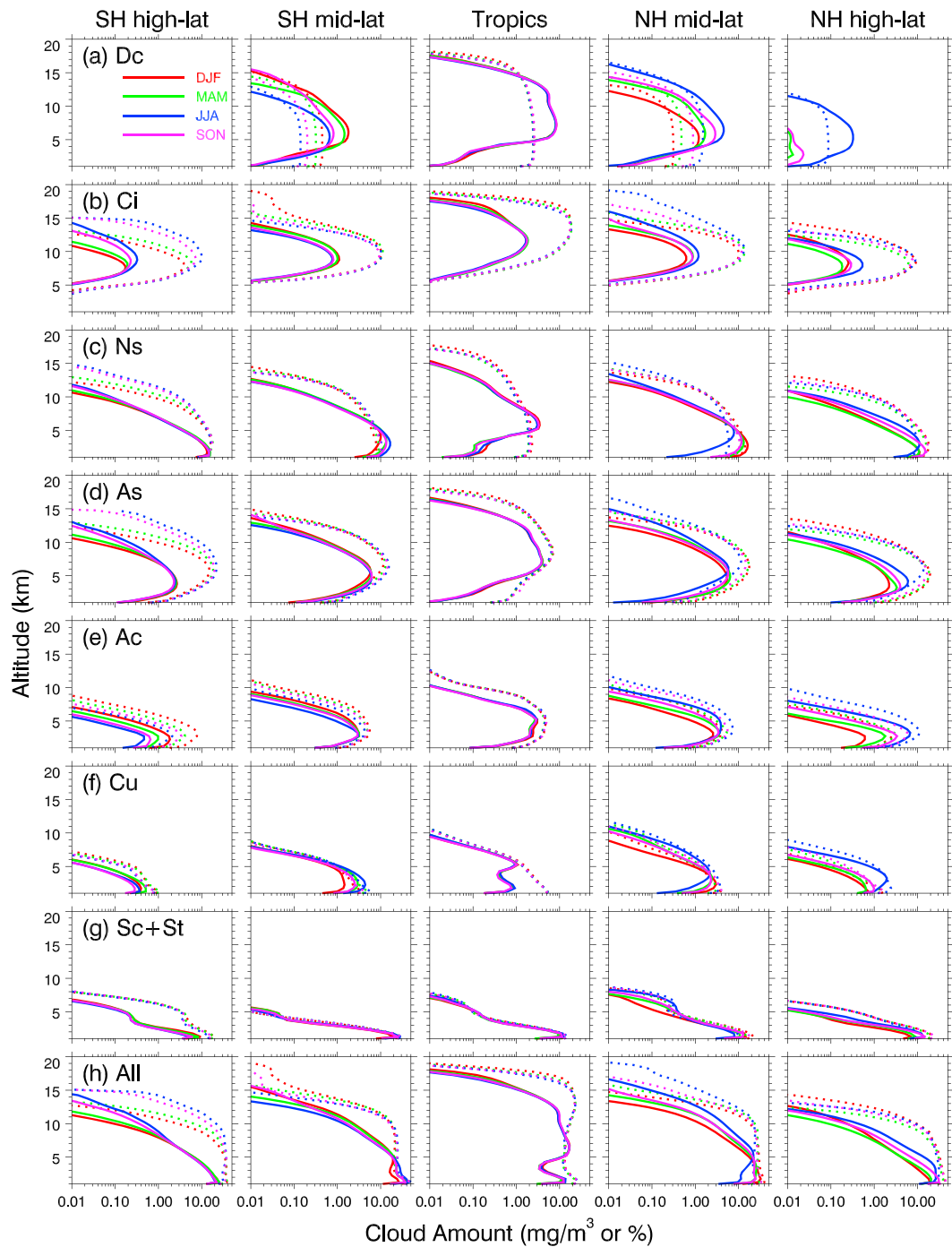


Figure 4. Vertical profiles of seasonal average cloud water content (solid line) and cloud fraction (dotted line) from 4 year CloudSat/CALIPSO observations over (first column) Southern Hemisphere (SH) high latitudes (60° – 82° S), (second column) SH middle latitudes (30° – 60° S), (third column) tropics (30° S– 30° N), (fourth column) Northern Hemisphere (NH) middle latitudes (30° – 60° N), and (fifth column) NH high latitudes (60° – 82° N) for each cloud type: (a) deep convective cloud, (b) cirrus, cirrocumulus, and cirostratus combined, (c) nimbostratus, (d) altostratus, (e) altocumulus, (f) cumulus, (g) stratocumulus and stratus combined, and (h) all types of cloud combined. The red color represents DJF season, green color represents MAM season, blue color represents JJA season, and purple color represents SON season.

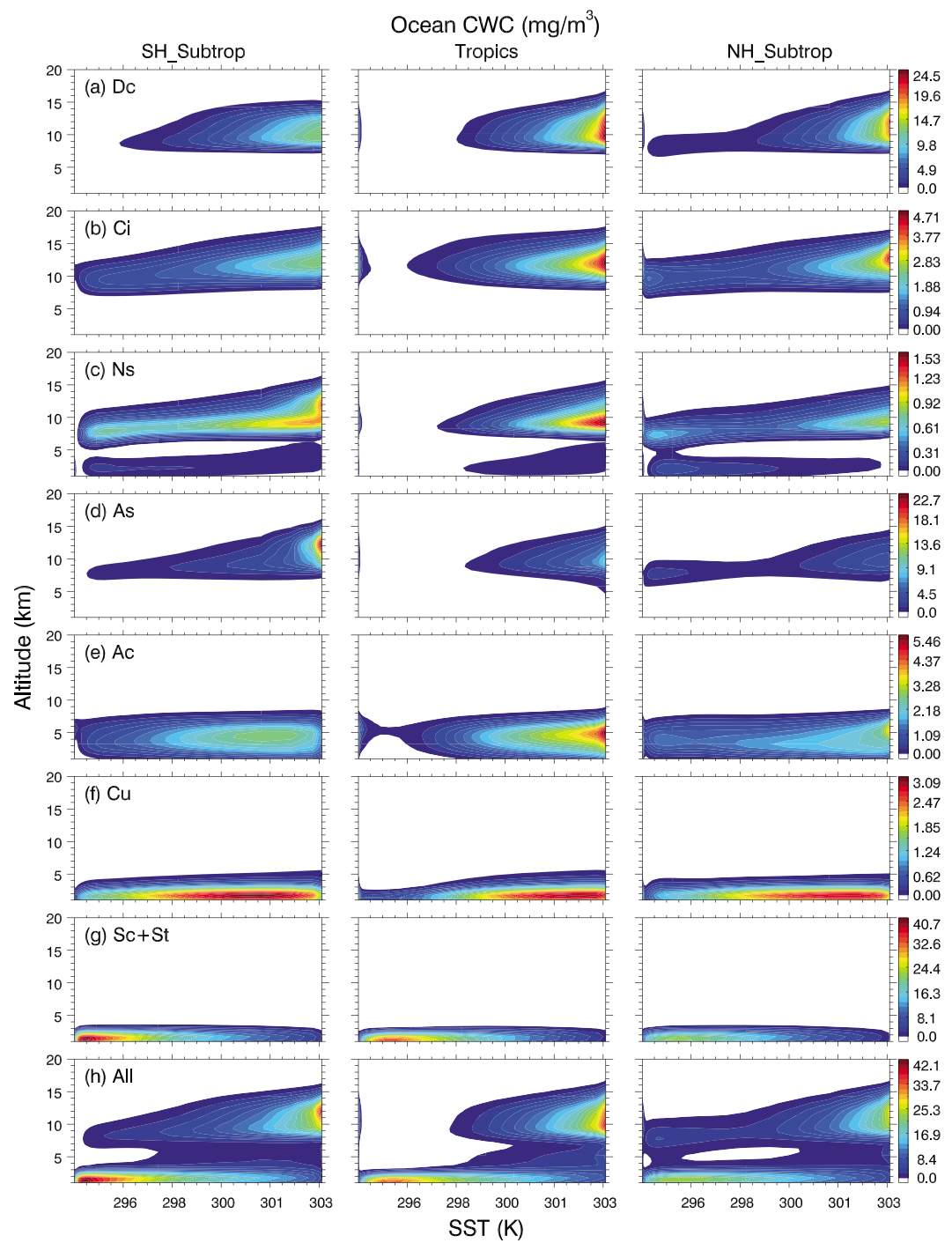


Figure 5. Vertical profiles of cloud water content (CWC, mg/m^3) from 1 year CloudSat/CALIPSO observations sorted by sea surface temperature (K) over the ocean area in the (left) Southern Hemisphere (SH) subtropics ($15^\circ\text{--}30^\circ\text{S}$), (middle) tropics ($15^\circ\text{S}\text{--}15^\circ\text{N}$), and (right) Northern Hemisphere (NH) subtropics ($15^\circ\text{--}30^\circ\text{N}$) for each cloud type: (a) deep convective cloud, (b) cirrus, cirrocumulus, and cirrostratus combined, (c) nimbostratus, (d) altostratus, (e) altocumulus, (f) cumulus, (g) stratocumulus and stratus combined, and (h) all types of cloud combined.

Over the high latitudes ($60\text{--}82^\circ\text{N}$ or $60\text{--}82^\circ\text{S}$), clouds in the NH also have larger seasonal variation than in the SH. However, the seasonal variations of most ice clouds are smaller than those over midlatitudes in the NH, due to less convective activity and lower atmospheric temperature. For example, Dc does not occur in the SH throughout the year, while it mainly occurs during JJA in the NH. Besides, the maximum altitudes that ice

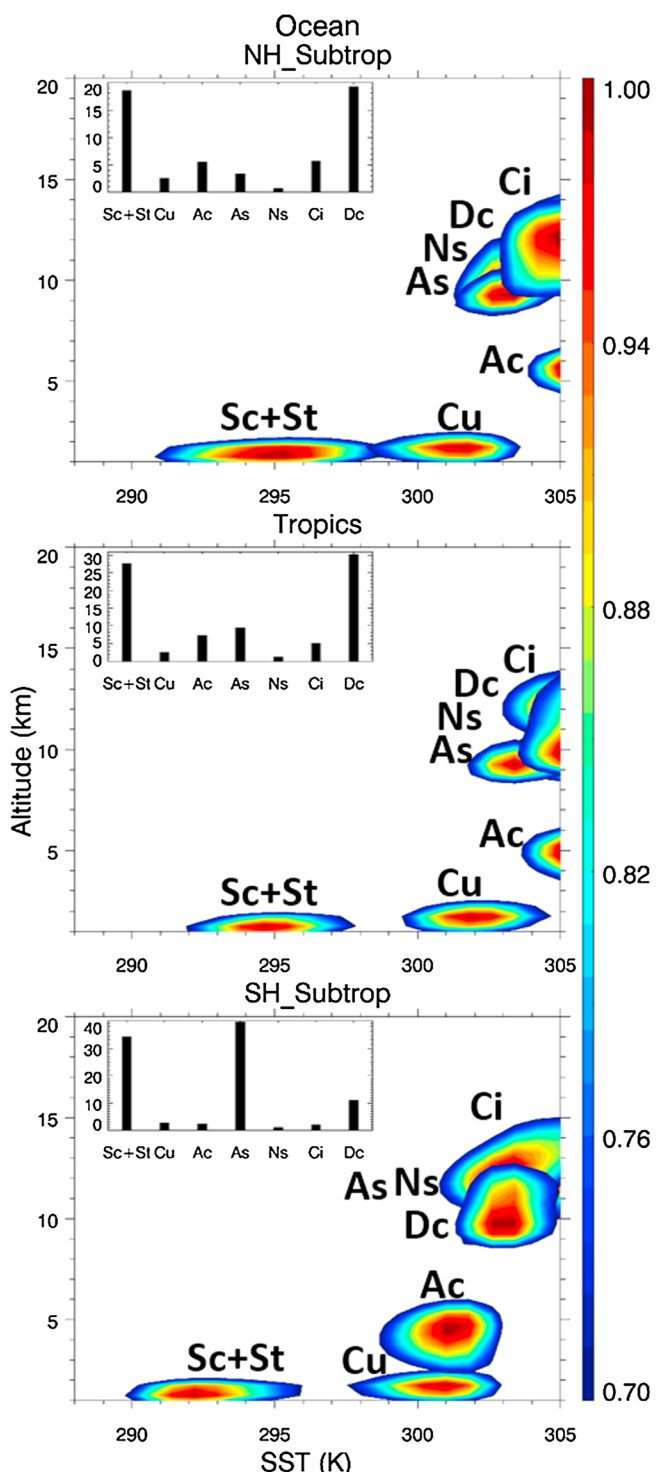


Figure 6. Vertical profiles of normalized cloud water content (CWC) of different cloud types from 1 year CloudSat/CALIPSO observations sorted by sea surface temperature (K) over the ocean area in the (top) Northern Hemisphere (NH) subtropics (15° – 30° N), (middle) tropics (15° S– 15° N), and (bottom) Southern Hemisphere (SH) subtropics (15° – 30° S). The bar chart within each panel shows the average of all the CWCs (mg/m^3) that are greater than 70% of the maximum CWC for each cloud type. See text for more details of the plotting method.

clouds can reach over high latitudes are much lower than over midlatitudes due to the lower tropopause height. In the NH, the large seasonal variations of ice clouds and Cu mainly occur in the middle troposphere and the CWCs reach maximum during JJA. In the SH, it is more complicated. Ci, Ns, and As have larger seasonal variations in the upper level than the lower level, and their CWCs and CFRs reach maximum during JJA. Ac has distinct seasonal variation from near surface to \sim 6 km, and its CWC and CFR reach maximum during DJF. Cu shows little seasonal variation in the SH. Similar to other latitudinal bands, Sc clouds have little seasonal variation in both hemispheres.

4. Relation Between Large-Scale Conditions and CWC Distribution

The above analyses have presented the climatologies of the vertical distributions of CWC and CFR for each cloud type and their seasonal variations over different latitudinal bands. It would be interesting to explore the relationships between large-scale environment conditions and the vertical distributions of these cloud types. The three parameters we selected in this study are SST, CAPE, and precipitation. All these parameters are derived from satellite observations colocated with CloudSat CWC measurements, thus they can represent the large-scale environment conditions when a type of cloud is observed by CloudSat.

Figure 5 shows the 1 year CWC profiles of each cloud type sorted by SST over three latitudinal bands (oceanic measurements only). Generally, the high clouds (Dc and Ci) show CWC peaks around 10 km in the warm SST (>300 K) regime, but their magnitudes are much different (Figures 5a and 5b). The CWC peak over the tropics is the largest, while the CWC peak over the NH subtropics is \sim 50% larger than that over the SH subtropics. For the middle clouds, Ns and As (Figures 5c and 5d) have CWC peaks between

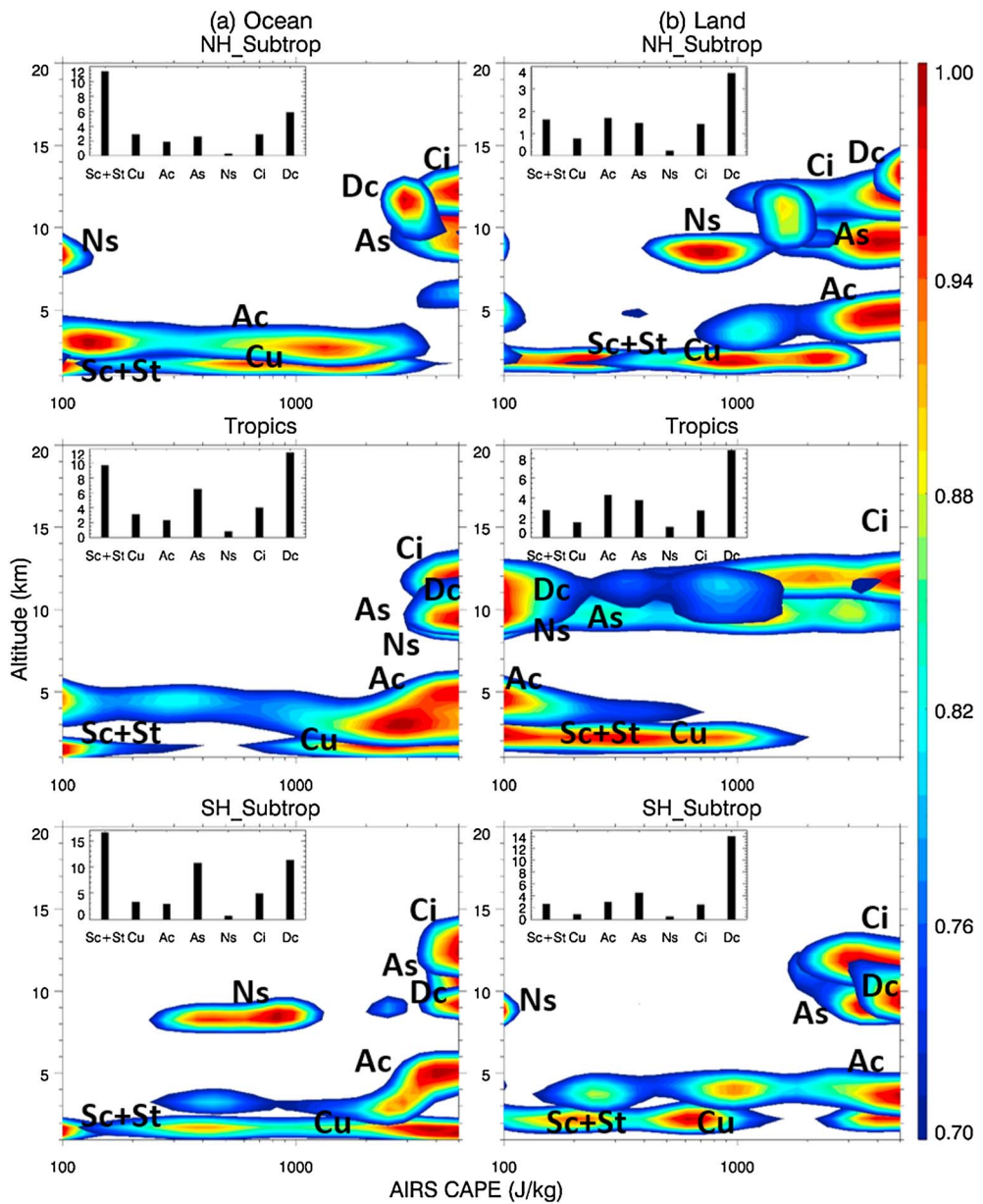


Figure 7. Same as Figure 6 but for CWC sorted by CAPE over the (a) ocean area and (b) land area.

5 km and 10 km, while the CWC peak of Ac (Figure 5e) is around 5 km. All the CWC peaks of these three types occur in the warm SST (>300 K) regime. Besides, there is a secondary CWC peak in the cool SST (<296 K) regime over the subtropics, especially in the NH. This may be caused by the intrusion of midlatitude storms into the subtropics [Su *et al.*, 2008]. Different from other types, Ns shows a two-layer mode of CWC distribution and the upper layer has larger CWC peak values than the lower layer. The relatively small CWC magnitude in the lower layer may be due to exclusion of precipitating clouds for LWC calculation. The CWC peak of Ac over the SH subtropics can extend to cooler SST (<298 K) regime. For the low clouds, although the CWC peaks of Cu and Sc are at approximately the same altitude, their locations in the SST regime are nearly opposite. Cu (Figure 5f) has a CWC peak in the warmer SST (>298 K) regime, while Sc (Figure 5g) has a CWC peak in the cooler SST (<298 K) regime. This is reasonable since Sc generally forms under stable environmental conditions that associated with low SST; on the other hand, Cu forms under unstable conditions. Besides, the CWC peak of Sc is about an order of magnitude larger than that of Cu, and its value in the SH is nearly twice as large as that in the NH, due to

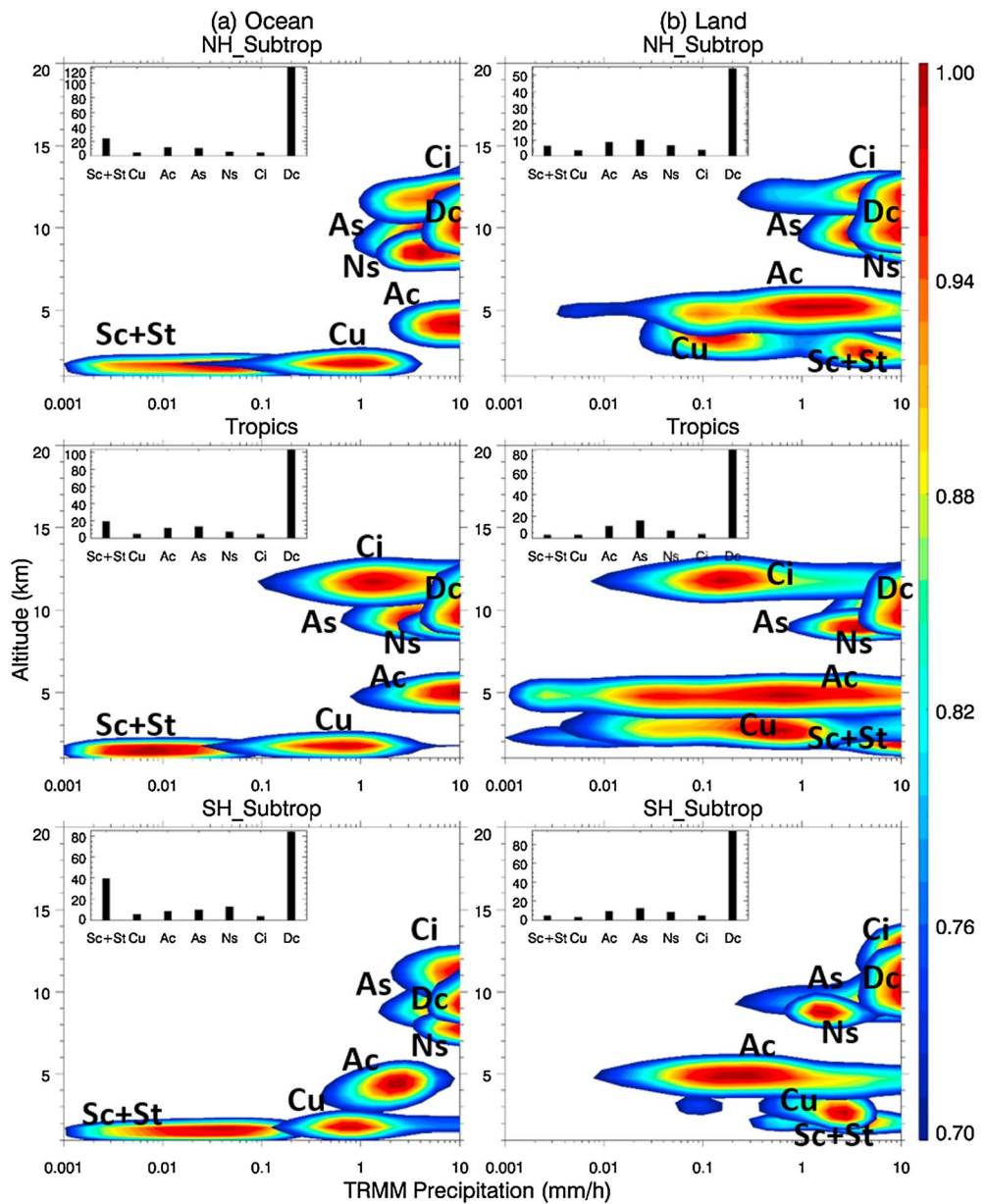


Figure 8. Same as Figure 6 but for CWC sorted by precipitation over the (a) ocean area and (b) land area.

higher occurrence frequency and larger spatial coverage. If we combine all types of cloud together (Figure 5h), it generally shows two modes: a deep mode with peak CWC higher than 7 km in the warm SST (>300 K) regime and a shallow mode with CWC peak below 2 km in the cool SST (<298 K) regime. The former is mainly contributed by Dc, Ci, and As clouds, while the latter is primarily contributed by Sc.

To better summarize the sorting results, we normalize the CWC using the maximum CWC value of each cloud type and show the results of all cloud types in one figure. We use 0.7 as a cutoff value for the normalized CWC. The average of all the CWCs that are greater than 70% of the maximum CWC for each cloud type is shown in a bar chart. Figure 6 is such an example of CWC sorted by SST over three latitudinal bands. It shows the relation between SST and the vertical distribution of large CWC ($>70\%$ of maximum value) for each cloud type. Generally, all the middle and high clouds have large CWCs in the warm SST (>303 K) regime at different altitudes. Ci is the highest (above 10 km); Dc, Ns, and As have some overlap at 8–10 km; Ac is the lowest (around 5 km). Cu and Sc clouds have large CWCs at 1–2 km, but the SST regime is totally different (299–303 K for Cu, <298 K for Sc). The magnitude of large CWCs for each cloud type varies with regions.

Over the NH subtropics and tropics, Dc and Sc clouds have the largest CWCs, while over the SH subtropics, As and Sc clouds have the dominant CWCs.

Using the same analysis method as in Figure 6, we also sort the CWC of each cloud type by CAPE and precipitation, and the results are shown in Figures 7 and 8, respectively. Over ocean area (Figure 7a), the large CWCs of Dc, Ci, and As are above 7 km in the high CAPE ($>2000 \text{ J/kg}$) regime; the large CWC of Ns does not have a consistent relation with CAPE over different latitudinal bands, and the magnitude is smallest ($<1 \text{ mg/m}^3$) among all cloud types. Ac has large CWC at ~5 km in the high CAPE ($>2000 \text{ J/kg}$) regime over SH subtropics and tropics. Over NH subtropics, the large CWC of Ac mainly occurs in the lower CAPE ($<2000 \text{ J/kg}$) regime. Cu and Sc clouds have large CWCs at 1–2 km, but their locations in the CAPE regime are totally different: Cu has large CWCs in a wide CAPE ($>200 \text{ J/kg}$) regime, while Sc has large CWCs in very low CAPE ($<200 \text{ J/kg}$) regime. Among all cloud types, Dc and Sc have dominant CWCs over the NH subtropics and tropics, while the CWCs of Dc, As, and Sc are much larger than other types over the SH subtropics. In contrast to ocean, the distributions of middle and high clouds over land are much different in the tropics (Figure 7b): Dc, Ci, and As have large CWCs in almost the entire CAPE regime, and the CWC magnitudes of As and Ac are comparable. For the low clouds, Cu and Sc have colocated large CWCs in a wide range of CAPE regime ($<1000 \text{ J/kg}$), although the CWC magnitude of Cu is smaller than that of Sc. Over land area, the CWC of Dc has the dominant magnitude among all cloud types over the three latitudinal bands, while the CWC magnitudes of Ci, As, Ac, and Sc are comparable.

Over ocean area (Figure 8a), the large CWCs of high and middle clouds (except Ac) are above 7 km in relatively high precipitation ($>1 \text{ mm/h}$) regime. Over the NH subtropics and tropics, large CWC of Ac is below 5 km in high precipitation ($>4 \text{ mm/h}$) regime; over the SH subtropics, it is in lower precipitation (1–4 mm/h) regime. For the low clouds, Cu and Sc clouds have large CWCs below 2 km, with Cu peaking in moderate precipitation (0.2–2 mm/h) regime and Sc peaking in low precipitation ($<0.2 \text{ mm/h}$) regime. Among all cloud types, Dc has the largest CWC magnitude ($>80 \text{ mg/m}^3$), Sc has the secondary largest magnitude ($20\text{--}40 \text{ mg/m}^3$), and Cu and Ci have the smallest ($<5 \text{ mg/m}^3$) magnitude over the three latitudinal bands. Over land area (Figure 8b), most of the middle and high clouds have similar CWC distributions to those over ocean area, but Ac and low clouds are quite different. Large CWC of Ac is in a wide range of precipitation ($>0.002 \text{ mm/h}$) regime; Cu and Sc have colocated large CWCs in high precipitation (1–6 mm/h) regime. The high precipitation associated with Sc may be artificial mainly due to two reasons: First, there could be other middle or high clouds (e.g., As) above Sc, thus the precipitation detected by TRMM may be produced by the clouds above Sc; second, CloudSat and TRMM have different orbits and observation time, which may cause mismatch in location and/or time between the two satellites' observations. This mismatch can have a larger impact on Sc over land since its occurrence frequency is much lower than that over ocean. Over land area, the CWC of Dc also has the dominant magnitude ($>80 \text{ mg/m}^3$) among all cloud types over the three latitudinal bands, while the CWC magnitudes of Ci, Cu, and Sc are the smallest and comparable ($<5 \text{ mg/m}^3$).

5. Conclusions

In this study, we present climatology of vertical distributions of cloud liquid water content (LWC), ice water content (IWC), and cloud fraction (CFR) associated with eight different cloud types, by using several CloudSat Level 2 products which include the combined CloudSat radar and CALIPSO lidar measurements. This is the first global climatology study of vertical IWC structure for different cloud types using radar-lidar combined data. The geographical and seasonal variations of these cloud properties for each cloud type are also analyzed, and their relationships with three parameters (SST, CAPE, and precipitation) derived from colocated satellite observations are investigated and discussed. The main findings of this study are summarized as follows:

5.1. Vertical Profiles of CWC and CFR

1. In general, ice-dominant clouds include As, Ns, Ci, and Dc; liquid-dominant clouds include Sc and St. For Ac and Cu, liquid (ice) phase dominates below (above) 7 km and 4 km, respectively.
2. Different cloud types have different altitudes of CWC and CFR peaks. The all-types-combined CWC profile shows two peaks: the one at 1–2 km is mainly contributed by Sc and the other one at 5–12 km is mostly contributed by Dc.

3. The peak of cloud fraction does not always overlap with that of CWC. Ci has the maximum CFR of 18% among the high clouds, As has the maximum CFR of 7% among the middle clouds, and Sc has the maximum CFR of 14% among the low clouds.
4. There is a clear asymmetric pattern of spatial distribution between NH and SH for nearly all types of cloud. The IWCs of high clouds reach maximum over the tropics and show an asymmetry on the two sides of the equator. Ice clouds are denser and can reach a higher altitude over the NH tropics than the south of equator. The maximum LWC and IWC of middle clouds mainly occur over middle-high latitudes of both hemispheres. The IWC of all three types (Ns, As, and Ac) is larger over the middle-high latitudes of SH than NH. As and Ac have larger IWC over the NH tropics than over the SH tropics. Ns has minimum CWC over the tropics and maximum CWC near surface over SH high latitudes. The low clouds have LWC peaks over the subtropics and extratropics and small IWC values in the polar regions. The CWC peak values of both Cu and Sc in the NH are much smaller than those in the SH.

5.2. Column-Integrated Cloud Water Path

1. For the distribution of cloud water path, the LWP is mostly contributed by Sc and St, while the IWP is mostly contributed by Dc over the tropics and Ns over the middle and high latitudes.
2. The largest LWPs of Sc and St are mainly located over the subtropical subsidence regions, such as the eastern Pacific, southern Atlantic, and south Indian Ocean. Ac has the second largest magnitude of LWPs, especially over the tropical convective regions.
3. The largest IWP values are associated with As, Ns, and Dc clouds, but the locations of the heaviest burden for these three types are quite different. Ci has little contribution to the global ice amount, with similar distribution of large IWPs to that of Dc. This may suggest that the detrainment of ice at the top of Dc plays an important role in the formation and distribution of Ci globally.

5.3. Seasonal Variation of CWC and CFR

1. Over the tropics (30°S – 30°N), all types of cloud show little seasonal variation of CWC and CFR.
2. Over both midlatitudes (30° – 60°N/S) and high latitudes (60° – 82°N/S), clouds have larger seasonal variation in the NH than in the SH, which is related to the land-ocean differences. Besides, Sc and St have little seasonal variation below 5 km. During wet season (i.e., JJA in the NH, DJF in the SH), both CWC and CFR of some ice clouds (Dc, Ci, As, and Ac) are larger than other seasons over the midlatitudes.
3. The seasonal variations of most ice clouds over high latitudes are smaller than those over midlatitudes in the NH, probably due to less convective activities. The maximum altitudes that ice clouds can reach over high latitudes are much lower than over midlatitudes.

5.4. Relationship With Environmental Parameters

When the CWC profiles of different cloud types are sorted by three parameters (SST, CAPE, and precipitation), each type of cloud shows distinct relationship with the environmental conditions.

1. Over ocean area, large CWCs of Dc, Ci, and As are above 7 km, and are associated with high CAPE ($>2000\text{ J/kg}$), warm SST ($>303\text{ K}$), and relatively high precipitation ($>1\text{ mm/h}$). Ci is the highest (above 10 km); Dc, Ns, and As have some overlap at 8–10 km; Ac is the lowest (around 5 km). Although both Cu and Sc clouds have large CWCs at 1–2 km, their locations in the three parameter regimes are totally different. Cu is generally associated with higher CAPE ($>200\text{ J/kg}$), warmer SST (299–303 K), and higher precipitation (0.2–2 mm/h), while Sc is mainly associated with lower CAPE ($<200\text{ J/kg}$), cooler SST ($<298\text{ K}$), and lower precipitation ($<0.2\text{ mm/h}$). Among all cloud types, Dc and Sc have dominant CWCs over all three latitudinal bands, but the CWC magnitude of As is also dominant over the SH subtropics in the SST and CAPE regimes.
2. Over land area, most of the middle and high clouds have similar CWC distributions compared to those over ocean area, but Ac and low clouds are quite different. Among all cloud types, Dc is the only type that has dominant CWC magnitude over all three latitudinal bands.

Clouds exert significant influences on the Earth's energy balance and the sensitivity of the climate system to various climate forcings [Stephens, 2005]; many of the key cloud properties related to these cloud impacts are governed by the vertical structure of clouds. Thus, this study provides useful results for many future cloud-impact studies, such as how aerosols interact with different types of clouds. It can also serve as a baseline observation to evaluate clouds simulated by global climate models.

Acknowledgments

This research is supported by the NASA AST, MAP, and CloudSat/CALIPSO programs. The study was performed at NASA Jet Propulsion Laboratory (JPL) at the California Institute of Technology, under contract with NASA. We thank Gerald G. Mace for useful discussions. We also appreciate the comments from three anonymous reviewers that led to significant improvements of this paper. The CloudSat Level 2 data sets are obtained from the CloudSat Data Processing Center, located at the Cooperative Institute for Research in the Atmosphere at Colorado State University. The SST data are obtained from the Remote Sensing Systems (<http://www.remss.com>). AIRS Level 3 products are obtained from AIRS Data Server (http://disc.sci.gsfc.nasa.gov/AIRS/data holdings/by-data-product-v5/airsL3_STD_AIRS_AMSU.shtml). TRMM precipitation data are obtained from GES DISC (<http://mirador.gsfc.nasa.gov/cgi-bin/mirador/homepageAlt.pl?keyword=3B42>).

References

- AghaKouchak, A., N. Nasrollahi, and E. Habib (2009), Accounting for uncertainties of the TRMM satellite estimates, *Remote Sens.*, 1, 606–619.
- Andrews, T., J. M. Gregory, M. J. Webb, and K. E. Taylor (2012), Forcing, feedbacks and climate sensitivity in CMIP5 coupled atmosphere–ocean climate models, *Geophys. Res. Lett.*, 39, L09712, doi:10.1029/2012GL051607.
- Austin, R. T., A. J. Heymsfield, and G. L. Stephens (2009), Retrieval of ice cloud microphysical parameters using the CloudSat millimeter-wave radar and temperature, *J. Geophys. Res.*, 114, D00A23, doi:10.1029/2008JD010049.
- Barker, H. W., A. V. Korolev, D. R. Hudak, J. W. Strapp, K. B. Strawbridge, and M. Wolde (2008), A comparison between CloudSat and aircraft data for a multilayer, mixed phase cloud system during the Canadian CloudSat-CALIPSO Validation Project, *J. Geophys. Res.*, 113, D00A16, doi:10.1029/2008JD009971.
- Bony, S., et al. (2006), How well do we understand and evaluate climate change feedback processes?, *J. Clim.*, 19, 3445–3482, doi:10.1175/JCLI3819.1.
- Chen, T., W. B. Rossow, and Y. Zhang (2000), Radiative effects of cloud-type variations, *J. Clim.*, 13, 264–286.
- Chen, W.-T., C. P. Woods, J.-L. F. Li, D. E. Waliser, J.-D. Chern, W.-K. Tao, J. H. Jiang, and A. M. Tompkins (2011), Partitioning CloudSat ice water content for comparison with upper tropospheric ice in global atmospheric models, *J. Geophys. Res.*, 116, D19206, doi:10.1029/2010JD015179.
- Deng, M., G. G. Mace, Z. Wang, and H. Okamoto (2010), Tropical composition, cloud and climate coupling experiment validation for cirrus cloud profiling retrieval using CloudSat radar and CALIPSO lidar, *J. Geophys. Res.*, 115, D00J15, doi:10.1029/2009JD013104.
- Deng, M., G. G. Mace, Z. Wang, and R. P. Lawson (2013), Evaluation of several A-Train ice cloud retrieval products with in situ measurements collected during the SPARTICUS campaign, *J. Appl. Meteorol. Climatol.*, 52, 1014–1030.
- Dong, X., B. Xi, and P. Minnis (2006), A climatology of midlatitude continental clouds from the ARM SGP central facility. Part II: Cloud fraction and surface radiative forcing, *J. Clim.*, 19, 1765–1783.
- Eliasson, S., S. A. Buehler, M. Milz, P. Eriksson, and V. O. John (2011), Assessing observed and modelled spatial distributions of ice water path using satellite data, *Atmos. Chem. Phys.*, 11, 375–391, doi:10.5194/acp-11-375-2011.
- Eriksson, P., et al. (2008), Comparison between early Odin-SMR, Aura MLS and CloudSat retrievals of cloud ice mass in the upper tropical troposphere, *Atmos. Chem. Phys.*, 8(7), 1937–1948, doi:10.5194/acp-8-1937-2008.
- Fetzer, E., et al. (2003), AIRS/AMSU/HSB validation, *IEEE Trans. Geosci. Remote Sens.*, 41, 418–431.
- Gentemann, C. L., T. Meissner, and F. J. Wentz (2010), Accuracy of satellite sea surface temperatures at 7 and 11 GHz, *IEEE Trans. Geosci. Remote Sens.*, 48(3), 1009–1018.
- Habib, E., and W. F. Krajewski (2002), Uncertainty analysis of the TRMM ground-validation radar-rainfall products: Application to the TEFLUN-B field campaign, *J. Appl. Meteorol.*, 41, 558–572.
- Harrison, E. F., P. Minnis, B. R. Barkstrom, V. Ramanathan, R. D. Cess, and G. G. Gibson (1990), Seasonal variation of cloud radiative forcing derived from the Earth Radiation Budget Experiment, *J. Geophys. Res.*, 95, 18,687–18,703, doi:10.1029/JD095iD11p18687.
- Hartmann, D. L., M. E. Ockert-Bell, and M. L. Michelsen (1992), The effect of cloud type on Earth's energy balance: Global analysis, *J. Clim.*, 5, 1281–1304.
- Haynes, J. M., T. S. L'Ecuyer, G. L. Stephens, S. D. Miller, C. Mitrescu, N. B. Wood, and S. Tanelli (2009), Rainfall retrieval over the ocean with spaceborne W-band radar, *J. Geophys. Res.*, 114, D00A22, doi:10.1029/2008JD009973.
- Heymsfeld, A. J., et al. (2008), Testing IWC retrieval methods using radar and ancillary measurements with in situ data, *J. Appl. Meteorol. Climatol.*, 47(1), 135–163, doi:10.1175/2007JAMC1606.1.
- Huang, L., R. Fu, J. H. Jiang, J. S. Wright, and M. Luo (2012), Geographic and seasonal distributions of CO transport pathways and their roles in determining CO centers in the upper troposphere, *Atmos. Chem. Phys.*, 12, 4683–4698, doi:10.5194/acp-12-4683-2012.
- Huang, L., J. H. Jiang, J. L. Tackett, H. Su, and R. Fu (2013), Seasonal and diurnal variations of aerosol extinction profile and type distribution from CALIPSO 5-year observations, *J. Geophys. Res. Atmos.*, 118, 4572–4596, doi:10.1002/jgrd.50407.
- Huang, L., R. Fu, and J. H. Jiang (2014), Impacts of fire emissions and transport pathways on the interannual variation of CO in the tropical upper troposphere, *Atmos. Chem. Phys.*, 14, 4087–4099, doi:10.5194/acp-14-4087-2014.
- Huffman, G. J., D. T. Bolvin, E. J. Nelkin, D. B. Wolff, R. F. Adler, G. Gu, Y. Hong, K. P. Bowman, and E. F. Stocker (2007), The TRMM Multisatellite Precipitation Analysis (TMPA): Quasi-global, multiyear, combined-sensor precipitation estimates at fine scales, *J. Hydrometeorol.*, 8, 38–55, doi:10.1175/JHM560.1.
- Jiang, J. H., et al. (2012), Evaluation of cloud and water vapor simulations in CMIP5 climate models using NASA "A-Train" satellite observations, *J. Geophys. Res.*, 117, D14105, doi:10.1029/2011JD017237.
- L'Ecuyer, T. S., and J. H. Jiang (2010), Touring the atmosphere aboard the A-Train, *Phys. Today*, 63(7), 36–41, doi:10.1063/1.3463626.
- Lazarus, S. M., S. K. Krueger, and G. G. Mace (2000), A cloud climatology of the southern Great Plains ARM CART, *J. Clim.*, 13, 1762–1775.
- Li, J. F., D. E. Waliser, and J. H. Jiang (2011), Correction to "Comparisons of satellites liquid water estimates to ECMWF and GMAO analyses, 20th century IPCC AR4 climate simulations, and GCM simulations", *Geophys. Res. Lett.*, 38, L24807, doi:10.1029/2011GL049956.
- Li, J.-L. F., et al. (2012), An observationally based evaluation of cloud ice water in CMIP3 and CMIP5 GCMs and contemporary reanalyses using contemporary satellite data, *J. Geophys. Res.*, 117, D16105, doi:10.1029/2012JD017640.
- Li, J.-L., et al. (2005), Comparisons of EOS MLS cloud ice measurements with ECMWF analyses and GCM simulations: Initial results, *Geophys. Res. Lett.*, 32, L18710, doi:10.1029/2005GL023788.
- Mace, G. G., R. Marchand, Q. Zhang, and G. Stephens (2007), Global hydrometeor occurrence as observed by CloudSat: Initial observations from summer 2006, *Geophys. Res. Lett.*, 34, L09808, doi:10.1029/2006GL029017.
- Mace, G. G., Q. Zhang, M. Vaughan, R. Marchand, G. Stephens, C. Trepte, and D. Winker (2009), A description of hydrometeor layer occurrence statistics derived from the first year of merged CloudSat and CALIPSO data, *J. Geophys. Res.*, 114, D00A26, doi:10.1029/2007JD009755.
- Randall, D. A., and S. Tjemkes (1991), Clouds, the Earth's radiation budget, and the hydrologic cycle, *Global Planet. Change*, 4(1–3), 3–9.
- Rossow, W. B., and R. A. Schiffer (1999), Advances in understanding clouds from ISCCP, *Bull. Am. Meteorol. Soc.*, 80, 2261–2286.
- Sassen, K. (1984), Deep orographic cloud structure and composition derived from comprehensive remote sensing measurements, *J. Climate Appl. Meteorol.*, 23, 568–583.
- Sassen, K. (1991), The polarization lidar technique for cloud research: A review and current assessment, *Bull. Am. Meteorol. Soc.*, 72, 1848–1866.
- Sassen, K., and Z. Wang (2008), Classifying clouds around the globe with the CloudSat radar: 1-year of results, *Geophys. Res. Lett.*, 35, L04805, doi:10.1029/2007GL032591.
- Sassen, K., and Z. Wang (2012), The clouds of the middle troposphere: Composition, radiative impact, and global distribution, *Surv. Geophys.*, 33, 677–691.
- Sassen, K., Z. Wang, and D. Liu (2009), Cirrus clouds and deep convection in the tropics: Insights from CALIPSO and CloudSat, *J. Geophys. Res.*, 114, D00H06, doi:10.1029/2009JD011916.

- Stephens, G. L. (2005), Cloud feedbacks in the climate system: A critical review, *J. Clim.*, **18**, 237–273.
- Stephens, G. L., et al. (2002), The CloudSat mission and the A-Train: A new dimension of space based observations of clouds and precipitation, *Bull. Am. Meteorol. Soc.*, **83**, 1771–1790.
- Stephens, G. L., et al. (2008), CloudSat mission: Performance and early science after the first year of operation, *J. Geophys. Res.*, **113**, D00A18, doi:10.1029/2008JD009982.
- Su, H., J. H. Jiang, D. G. Vane, and G. L. Stephens (2008), Observed vertical structure of tropical oceanic clouds sorted in large-scale regimes, *Geophys. Res. Lett.*, **35**, L24704, doi:10.1029/2008GL035888.
- Su, H., et al. (2011), Comparison of regime-sorted tropical cloud profiles observed by CloudSat with GEOS5 analyses and two general circulation model simulations, *J. Geophys. Res.*, **116**, D09104, doi:10.1029/2010JD014971.
- Su, H., et al. (2013), Diagnosis of regime-dependent cloud simulation errors in CMIP5 models using “A-Train” satellite observations and reanalysis data, *J. Geophys. Res. Atmos.*, **118**, 2762–2780, doi:10.1029/2012JD018575.
- Su, H., J. H. Jiang, C. Zhai, T. J. Shen, J. D. Neelin, G. L. Stephens, and Y. L. Yung (2014), Weakening and strengthening structures in the Hadley Circulation change under global warming and implications for cloud response and climate sensitivity, *J. Geophys. Res. Atmos.*, **119**, 5787–5805, doi:10.1002/2014JD021642.
- Waliser, D. E., et al. (2009), Cloud ice: A climate model challenge with signs and expectations of progress, *J. Geophys. Res.*, **114**, D00A21, doi:10.1029/2008JD010015.
- Wang, Z., and K. Sassen (2001), Cloud type and macrophysical property retrieval using multiple remote sensors, *J. Appl. Meteorol.*, **40**, 1665–1682.
- Wang, Z., et al. (2013), *CloudSat Project: Level 2 Combined Radar and Lidar Cloud Scenario Classification Product Process Description and Interface Control Document*, 61 pp., California Institute of Technology, Calif.
- Winker, D. M., W. H. Hunt, and M. J. McGill (2007), Initial performance assessment of CALIOP, *Geophys. Res. Lett.*, **34**, L19803, doi:10.1029/2007GL030135.